Nonmonotonic spatial profiles of excitation rates in bounded plasmas caused by effects of EDF nonlocality

E. A. Bogdanov, A. A. Kudryavtsev, L. D. Tsendin*,

St. Petersburg State University, St. Petersburg, 198504 Russia, E-mail: akud@ak2138.spb.edu
** St. Petersburg State Polytechnic University, St. Petersburg, 195251 Russia*

It is shown that the influence of the nonlocal character of the EDF on the spatial profiles of of excitation rates is essential up to high gas pressures *pR<100 cmTorr*. A paradoxical effect related to the nonlocal character of the EDF revealed: the peaks of the profiles of the excitation rates shift from the discharge axis toward the periphery as the pressure increases. This effect cannot be understood from the hydrodynamic point of view and it is related to the nonlocal character of the electron distribution function.

When simulating gas-discharge plasma, the electron distribution function (EDF) is usually calculated on the traditional local approximation [1,2]. This means that terms with both spatial gradients and the ambipolar electric field are omitted in the kinetic equation and the EDF is factorized as

$$f_0(w,x) = n_e(r) f_0^0(w, E/p) \qquad (1)$$

In this approximation, the electron distribution over the kinetic energy $w = m v^2/2$ at a fixed point x depends on the local parameters; first of all, from the heating electric field intensity *E*. The inhomogeneity results in small corrections which determine particle and (if necessary) energy fluxes which are proportional to the relatively small gradients of these parameters. They manifest themselves in the formation of fluxes of particles and energy which are proportional to these gradients. Such an approach is characteristic for the plasma transport theory (the so-called fluid approach, see for example [1-3]). In this approximation the direction of the differential fluxes (i.e. of the contributions of different EDF parts to the total particle and energy fluxes) coincide with the direction of the total fluxes. Correspondingly, the rates of electron collisions, f.e. impact excitation rates

$$W_k(x) = 4\pi \int_{\varepsilon_k}^{\infty} f_0(v,x) \nu_k(v) v^2 dv = \nu_k(E/p) n_e(x), \qquad (2)$$

of neutral levels *k*, which control plasmachemical reaction rates, plasma luminousity and composition, ionization, etc., is proportional to the electron density $n_e(x)$ [1,2]. In other words, the excitation frequencies $\nu_k(E/p)$ are determined by the local EDF f_0^0 which depends on the local values of the heating electric field intensity and other parameters (the gas temperature, the density of excited particles, etc.). Consequently, in gas discharge plasmas this field is the dominant factor which controls spatial $W_k(x)$ profiles, and they are expected to reproduce the heating field and the electron density profiles. Therefore in a DC positive column plasmas, where electrons are heated by the uniform longitudional electric field E_z, nobody to our knowledge can doubt, that all the excitation rates in a positive column are to be maximal at the tube axis, where the plasma density is maximal. Nevertheless, in simulations [9,10] of the positive column (PC) in Ar, the surprizing phenomenon revealed, that excitation rates were maximal not at the tube axis, but somewhere at its periphery up to pressures $pR = 100$ *cmTorr*. Thereupon applicability of local approximation for EDF calculations requires careful inspection.

Traditional local approach to be applicable only when terms with spatial gradients can be omitted in the kinetic equation, i.e. the electron energy relaxation length λ_ε is negligible quantity [4]. In the opposite case the EDF is of nonlocal nature; i.e., it depends on the values of the physical parameters (primarily on the field strength) in the region determined by the inequality $\lambda_\varepsilon >> \lambda$ (where λ is the electron mean free path), rather than on their values at a given point. At estimation of the λ_ε it is necessary to take into account that the relation between the volume processes and the diffusion of electrons onto the walls can be different for different electron energy ranges.

If the electron energy balance is determined by elastic collisions, then for atomic gases in the energy range $\varepsilon < \varepsilon^*$ - the threshold energy for inelastic processes, in which most electrons are concentrated, electron energy relaxation length is

$$\lambda_\varepsilon \simeq \sqrt{D_r/(\delta\nu)} \simeq \lambda/\sqrt{\delta} > 100\lambda \qquad (3)$$

(here, $D_r = \lambda V/3$ - is the coefficient of spatial electron diffusion and $\delta = 2m/M$). When $\lambda_\varepsilon > \Lambda$ - characteristic diffusion length, the EDF is nonlocal throughout the whole plasma volume. Length (3) is more than two orders of magnitude larger than the electron mean free path and inequality $\lambda_\varepsilon > \Lambda$ is satisfied up to relatively high pressures $p\Lambda \le (5-10)\,cmTorr$.

Since at $\lambda_\varepsilon > \Lambda$, the energy of an electron during its single pass across the discharge volume changes only slightly, the integral of motion of such electrons is the total energy (the kinetic energy plus the potential energy)

$$\varepsilon = w + e\varphi(r) = m v^2/2 + e\varphi(r) \qquad (4)$$

In the energy range $\varepsilon > \varepsilon^*$, which corresponds to inelastic collisions, an electron diffuses on the distance corresponding electron energy relaxation length

$$\lambda_\varepsilon^* = \sqrt{D_r/\nu^*} \simeq \sqrt{\lambda\lambda^*} \simeq (3-10)\lambda \qquad (5)$$

over its characteristic lifetime ($\sim 1/\nu^*$) (here, $\lambda^* = 1/(N\sigma^*)$ is the electron mean free path in inelastic processes). The length λ_ε^* (5) is much shorter than λ_ε that given by Eq. (3).
Therefore, from the physical standpoint, the most appropriate arguments for describing a nonlocal EDF are the variables ε and r [3,4].

Because of the presence of two very different energy scales, the nonlocal character of the EDF manifests itself in different ways in its different parts. In terms of the total energy (4), the nonlocal EDF can be either dependent on or independent of the radius [4]. The most examined marginal case of low pressures when $\lambda^*_\varepsilon > \Lambda$ and as the body and so tail of the EDF at $\varepsilon \le e\Phi_w$ depend only on the total energy ε [4-6] (Φ_w is the potential difference between the discharge axis and the tube wall). At higher pressure, when inequality $\lambda_\varepsilon > \Lambda > \lambda_\varepsilon^*$ holds, the situation becomes more diverse [7-9]. In this case the EDF body at $\varepsilon < \varepsilon^*$ remains a function on ε only, but the EDF tail, at $\varepsilon > \varepsilon^*$, depends both on ε and *x*. This case begin to analyse only recently [7-11] and many surprising phenomena are discovered and expected. One of the most impressive is the case of paradoxical non-monotonic behavior of excitation rates spatial profiles in DC positive column plasmas [9-11].

In this paper we present the main results, their concise explaination and scalings for the excitation profiles in a PC at moderate and high pressures.

The positive column (PC) plasma is the most studied object of the low-temperature plasma physics. Relative simplicity of its creation and diagnostics makes it traditional benchmark and testing

field for vast majority of novel concepts and approaches. In [9,10] it was pointed out that above mentioned paradoxical phenomena of non-monotonic behavior of excitation rates spatial profiles are caused by the non-local electron kinetics [4] and in [11] was presented a kinetic analysis of the problem.

The simulation code used in this work in described in detail in [12]. The code solves continuum equations for various plasma species coupled with Poisson equation for the electrostatic field. Heavy particles were described in the fluid model.The electron energy distribution function is calculated by solving the Boltzmann equation using two-term spherical harmonics expansion. For EEDF calculations, we have accounted for various processes including stepwise excitation and ionization, as well as the generation of energetic electrons in collisions of the second kind with metastables and Penning ionization between metastables. At the tube wall $r=R$, the loss-cone boundary condition has been used (see e.g., [6,7]). We consider six plasma species: *Ar* (ground state), *Ar**, and *Ar*** (two metastable states with energies $\varepsilon^{*}=11.55\ eV$ and $\varepsilon^{**}=13.2\ eV$, correspondingly), Ar_r^{*} (resonance state), Ar^{+}, and Ar_2^{+} (atomic and molecular ions). The argon chemistry mechanism is similar to that used in [13]. It includes conversion of atomic to molecular ions and so can be used in a wide range of gas pressures. The mechanism consists of 21 steps including various electron-induced excitation and ionization steps, and radiation transitions from *Ar*** to *Ar** states and from Ar_r^{*} to *Ar* (radiation trapping is accounts for both Doppler and collisional line broadening).
The calculated radial profiles of excitation rates R_1 and R_2 for the reactions $Ar+e \leftrightarrow Ar^{*}+e$ and Ar+e↔Ar**+e are shown in Fig. 1 for different gas pressures. Off-axis peaks of both excitation rates are observed for a pressure range $5<p<50$ Torr. The R_2 peaks (Fig. 1b) are more pronounced than the R_1 peaks [Fig. 1(a)]. The nonmonotonic excitation rates result in nonmonotonic distributions of excited species. For example, Fig. 2 shows the radial profiles of Ar* density at different gas pressures. One can see that *Ar** density is nonmonotonic at pressures from 5 to 50 Torr. The densities of other excited species have similar radial profiles. The electron density profiles are close to Bessel distributions with the maximum values varying from $1.6\times10^{9}\ cm^{-3}$ (at *1 Torr)* to $1.5\times10^{10}\ cm^{-3}$ (at *100 Torr*). The axial electric field E_z calculated self-consistently by the code has values *6.9, 6.2, 12.1, 31.3, 64.9, and 131.7 V/cm for p=1, 5, 10, 25, 50, and 100 Torr,* for the fixed discharge current of *1 mA*. For such a low current, Coulomb collisions, volume recombination, and gas heating are not important. Thus, the observed effect cannot be understood from the hydrodynamic point of view and their understanding can be achieved by analysis of electron kinetics in PC at moderate gas pressures.

Let us give a kinetic analysis of the problem for the excitation profiles in a PC. In order to clarify the underlying physics, here we would consider the model problem for the plane-parallel geometry with the gap spacing *2L*.

The kinetic equation in variables coordinate *x* and the total electron energy ε (4) takes the form (see, for example, [4,11]):

$$\frac{1}{r}\frac{\partial}{\partial r}\left(r\sqrt{w}D_r\frac{\partial f_0}{\partial r}\right)+\frac{\partial}{\partial\varepsilon}\left(\sqrt{w}\left(D_E\frac{\partial f_0}{\partial\varepsilon}+V_{ea}f_0\right)\right)= \sum_k\left(\nu_k(w)\sqrt{w}f_0(\varepsilon)-\sum_k\nu_k(w+\varepsilon_k)\sqrt{w+\varepsilon_k}f_0(\varepsilon+\varepsilon_k)\right)-\frac{n_m g_a \nu_{ex}(w)\sqrt{w}}{N_0 g_m}f_0(\varepsilon-\varepsilon^{*}) \quad (6)$$

This equation accounts for both the longitudional E_z and transversal $E_x = -\varphi_x'(x)$ electric fields. $D_r = \lambda V/3$ is the spatial diffusion coefficient, and $D_E = (eE)^2 D_r$ is the diffusion coefficient along the energy axis, which relates to the Joule heating by the field. The energy loss in the elastic collisions results in the "velocity" along the energy axis $V_{ea} = w\delta\nu$. The right-hand side of Eq. (6) includes sources and sinks due to inelastic processes. Here, ν_k corresponds to the inelastic collisions with excitation of an atomic level *k*; the first term is nonzero only at the EDF tail, when $w > \varepsilon_1$; (in the region III in Fig.3a); the second one, which desribes the electrons appearing after an inelastic collision with small energy; is important only at small energies (in the region I in Fig. 3a); we would neglect it later on. The last one, which desribes the electrons appearing after an superelastic collisions of electrons with long-living metastable atoms $Ar^* + e \; Ar + e$, when slow bulk electron additionally acquires the threshold excitation energy * and instantaneously becomes fast. These processes substantially influence the calculated values of the constants for the excitation reactions with high threshold energies and, accordingly, the densities of highly excited states (see [10] for details). ν_{ex} is the excitation frequency of the metastable level.

The kinetic equation (6) is the *2D* diffusion equation with with ε and *x*, as arguments. It is reasonable to introduct the fluxes along the energy axis and along the transversal (radial) coordinate:

$$\Gamma_\varepsilon = -\left(D_E(w,x)\frac{\partial f_0}{\partial \varepsilon} + V_{ea}(w) f_0 \right) \qquad (7a)$$

$$\Phi_x = -D_r(w)\frac{\partial f_0}{\partial r} \qquad (7b)$$

At moderate and higher pressure, when $\lambda_\varepsilon > \Lambda > \lambda_\varepsilon^*$, as it was already mentioned, the EDF body at $\varepsilon < \varepsilon^*$ remains a function on ε only, but the EDF tail, at $\varepsilon > \varepsilon^*$, depends both on ε and x. When kinetic energy $w = \varepsilon - e\varphi(x) > \varepsilon^*$ is enough for inelastic collision (region *III* in Fig.3), the EDF decreases sharply, $\sim \exp(-\varepsilon/T^*)$; $\sim \exp(-x/\lambda_\varepsilon^*)$, where

$$T^*(\varepsilon) \simeq (D_\varepsilon/\nu^*)^{1/2} = eE_z\lambda_\varepsilon^* \qquad (8)$$

is the electron "temperature in inelastic region. The electrons with $w > \varepsilon^* + T^*$ are practically missing. In the region *IIb* (see Fig.3a) inelastic collisions are absent and their influence results in intense inward directed differential spatial flux $\Phi_x(\varepsilon, x)$ (the diffusive flux of electrons with given total energy) is formed in the region *IIb* (see Fig.3a) and zero condition for the EDF ("black wall" approximation) can be imposed at the boundary between the regions *IIb* and *III*, which is given as

$$e\varphi(x^*(\varepsilon)) = \varepsilon - \varepsilon^* \qquad (9)$$

If $L >> \lambda_\varepsilon^*$ the expression (2) for the total excitation rate can be considerably simplified. The spatial differential flux Φ_x, and the flux along the energy axis Γ_ε are shown in Fig 3a. The excitations occur in the narrow ($\sim T^*$) strip in the (ε, x) plane (dotted in Fig.3b) Multiplying (6) by $(4\pi V^2 dV dx)$ and integrating it over the srip, which length Δx satisfies conditions

$$L >> \Delta x >> \lambda_\varepsilon^* \qquad (10)$$

we obtain:

$$W_{ex}(x)\Delta x = -\frac{4\pi}{m}V\Delta x\left[\Gamma_\varepsilon + \frac{\Delta\varepsilon}{\Delta x}\frac{\partial f_0}{\partial x}\right] = -\frac{4\pi}{m}V\Delta x\left[D_\varepsilon\frac{\partial f_0}{\partial \varepsilon} + D(eE_r)\frac{\partial f_0}{\partial x}\right] \qquad (11)$$

The first term in the expression for the excitation rate (11) corresponds to the traditional mechanism of the Joule heating (diffuson along energy). It is maximal at the gap midplane. Since the EDF in the region IIb (see Fig.3a) decreases exponentially with energy, the corresponding contribution to the exitation rate (2) decreases towards the column periphery.

The second term relates to the spatial diffusive differential flux Φ_X that is inward-directed in the region IIb (see Fig.3a). Since this flux describes the diffusion with ε conservation, the kinetic energy of the electrons in the range $\varepsilon^* < \varepsilon$ increases. In other words, these electrons are "heated" by the radial electric field. It is to be noted that in our approximation the total electron transversal flux equals zero (the flux Φ_ε in IIa is outward directed, Fig.3a, and compensates the inward-directed flux in IIb). That is why this effect cannot be treated in the conventional terms of the fluid approximation (see [7] for details). This spatial term is proportional to

$$\Delta\varepsilon = eE_x\Delta x \qquad (12)$$

and equals zero both at $x=0$ and at $x \to L$; the peripherically peaked $W_{ex}(x)$ profiles arise, if this term dominates.

At $\lambda_\varepsilon > L$ the term V_ε in (6) mostly can be neglected in the region IIb. So we have an estimate for the excitation rate profile

$$\frac{W_{ex}(x)}{W_{ex}(0)} = \left[\frac{\partial f_0(x,\varepsilon)}{\partial\varepsilon} + \frac{E_x}{(eE_Z)^2}\cdot\frac{\partial f_0(x,\varepsilon))}{\partial x}\right]\Bigg|_{\varepsilon=e\phi(x)+\varepsilon_1} \times \left(\frac{\partial f_0}{\partial\varepsilon}\Big|_{x=0,\varepsilon=\varepsilon_1}\right)^{-1} \qquad (13)$$

We performed estimates of the rate profile (13) using the WKB solution for the EDF in the region IIb that was formulated in [7]. This solution satisfies zero boundary conditions for the function f_0 at $x = x^*(\varepsilon)$ (9), and for its spatial derivative at $x = L$, and is exponentially decreasing with ε [7]

$$\begin{aligned} f_0(x,\varepsilon) &\sim \exp\left[-\Psi(\varepsilon)\right]\sin\left[\frac{\pi}{2}\frac{(x-x^*(\varepsilon))}{(L-x^*(\varepsilon))}\right]; \\ \Psi(\varepsilon) &= \frac{\pi}{2}\int_{\varepsilon_1}^{\varepsilon}\sqrt{\frac{D}{D_\varepsilon}}\frac{d\varepsilon'}{\left(L-x^*(\varepsilon)\right)} \approx \frac{\pi}{2}\frac{(\varepsilon-\varepsilon_1)}{eE_Z(L-x^*(\varepsilon))}. \end{aligned} \qquad (14)$$

The first term in the numerator in (13) decreases with x due to EDF decrease along the boundary between the regions III and IIb. On the contrary, the second one is zero at $x = 0$. It rises at small x values due to the $E_x(x)$ rise. At larger x values the exponential decrease of the EDF $f_0(x, \varepsilon = \varepsilon_1 + e\phi(x))$ (see (14) overcomes this factor, and so this term has a maximum at some $x \neq 0$. The estimate of (13) yields

$$\frac{W_{ex}(x)}{W_{ex}(0)} \approx \exp\left[-\frac{\pi}{2}\frac{\phi(x)}{E_Z(L-x)}\right]\cdot\left(1+\frac{E_x}{E_Z}\right). \qquad (15)$$

The effect can be interpreted in terms of an electrostatic analogy (Fig. 4). At $V_\varepsilon \to 0$ and neglecting the last term in the right-hand side of (6), in the absorbing wall approximation, the problem is to find the Laplace equation solution, with the EDF $f_0(\varepsilon, x)$ analogous to the electrostatic "potential" which is created by the uniformly charged plane at $\varepsilon = 0$, the boundary between *III* and *IIb* is analogous to the conducting surface, and the excitation rate is analogous to the surface charge per unit length along the *x* axis *σ(x)*. The boundary condition of zero flux at the vessel wall can be interpreted as the periodicity condition along *x*. So, it is obvious that if some parts of the conducting

surface are normal to *x*, the surface charge per unit length along the x axis tends to infinity there. On the contrary, if the conducting urface is smooth enough, the surface charge on the conductor per unit length along *x* is maximal at the points where ε at the conductor surface is minimal.

If ambipolar potential is approximated, as

$$e\phi(x) = -a\,\varepsilon_1 (x/L)^n / n\,, \tag{16}$$

it is easy to derive the algebraic equation for maximum position x_0 of (15). If $A = \varepsilon_1 /(eE_Z L) \gg 1$ then value of x_0 can be estimated as:

$$x_0 = \sqrt[n]{n/(\pi A a)} \tag{17}$$

The formulated considerations are illustrated for the model problem for the plane-parallel geometry with *2L=2 cm* . For $\phi(x)$ we had used approximation (16) with $n = 2{,}3$.

The spatial profiles of the excitation rate $W_{ex}(x)$ (2) are presented in Fig. 5 for $E_Z / p = const$ and different pressures p [11]. It can be seen that at low pressure, when the whole EDF is nonlocal, the total excitation rate is peaked at the plasma center (curve A). In contrast at moderate pressure the peak of the $W_{ex}(x)$ (curves B, C) is substantially displaced from the PC axis. The x_0 position for curves B and C obtained from (15), (16) are 0.33 and 0.38 accordingly; These values are in agreement with numerical results (Fig.4): 0.41 and 0.55. At higher pL values $\lambda_\varepsilon < L$ and EDF in the whole region II becomes local. Nevertheless, the nonlocal effects still exist at distance λ_ε from the wall, if the potential profile $\phi(x)$ in the wall vicinity is steep enough. It can be seen from curve D that the $W_{ex}(x)$ profiles in the central vessel part are maximal at $x = 0$, but at the distance from the wall of the order of $\lambda_\varepsilon = \sqrt{M/m}\,\lambda$, where the EDF is non-local, the satellite maximum remains. If the $\phi(x)$ profile is more smooth (say, for *n=3/2* in (15)), the satellite maximum disappears.

The quick test for existence of nonmonotonic profiles and maximum position is the exceeding the value of radial field E_x compeare to external (axial) field E_z (see (13,15). Therefore for effect presence the profile of radial potential should be rather steep. In Fig. 6 the excitation rate spatial profiles $W_{ex}(x)$ are presented in dependence of E_x. In the absence of the transversal electric field the dependence of total excitation frequency $W_{ex}(x) = const(x)$. At low E_x it is maximal at $x = 0$; at higher E_x the maximum is shifted towards to the periphery.

Since the destruction rate of metastable atoms (which is determined by the mixing to a neighboring resonance level) is a smooth function of *x*, the nonmonotonic behavior of the production rate of these atoms leads to nonmonotonic $N_m(x)$ profiles (see Fig.2) [9-11].

The excitation rates of individual levels $W_k(x)$ with the excitation energies ε_k can be divided roughly into two groups.

The excitation rates for the levels with the low ε_k, for which the excitation threshold satisfies condition $\varepsilon_k < \varepsilon^* + T^*$, i.e. lies within the dotted strip in the Fig.3b, the excitation rates behave, roughly speaking, in a similar way, as in (15).

The spatial profiles of the higher levels excitation rates with the threshold is given by $\varepsilon_k > T^*$ (Fig.7) are considerably more depend on EDF in region *III*. Electrons in the axial region cannot gain energy $\varepsilon > \varepsilon_k$ in the electric field if they previously did not undergo inelastic collisions with lower levels because $\varepsilon_k - \varepsilon^* > T^*$. On the other hand, they cannot reach the axis due to radial diffusion

because $\lambda_\varepsilon^* << R$. In other words, an electron with energy ε can most easily reach the region with $w > \varepsilon_k$ as follows: First, the electron diffuses over energy up to $\varepsilon > \varepsilon_k$ at the periphery of the plasma column, where the kinetic energy is low $\varepsilon - e\varphi(r) < \varepsilon^*$ and the electron does not undergo inelastic collisions. Then, this electron diffuses in the radial direction toward the axis over a distance $\sim \lambda_\varepsilon^*$. For this reason, the maximum excitation rate (and the corresponding rate constant) of the level ε_k is shifted from the curve $r = r_k(\varepsilon)$ (where $\varepsilon - e\varphi(r_k(\varepsilon)) = \varepsilon_k$) by λ_ε^* toward the axis.

The values of $W_{ex}(x)$ depend most crucially on the exponentially small probability to overcome the absorbing region between the curves $\tilde{x}^*(\varepsilon)$ and $\tilde{x}_k^*(\varepsilon)$ in Fig.7. In order to estimate this probability, note that in the dimensionless units

$$\tilde{x} = x\sqrt{\nu^* / D} = x / \lambda_\varepsilon^*, \qquad (18)$$
$$\tilde{\varepsilon} = \varepsilon \sqrt{\nu^* / D_\varepsilon} = \varepsilon / T^*,$$

assuming vD, vD_ε, $v\nu^*$ to be velocity-independent, we have for kinetic equation (6) in the region *III*:

$$\frac{\partial^2 f_0}{\partial \tilde{\varepsilon}^2} + \frac{\partial^2 f_0}{\partial \tilde{x}^2} = -f_0. \qquad (19)$$

The excitation rates $W_k(x)$ are maximal at the points $\tilde{x} = \tilde{x}_1$, where the "absorbing barrier" between the curves $\tilde{x} = \tilde{x}^*(\varepsilon)$, and $\tilde{x} = \tilde{x}_k^*(\varepsilon)$ is most transparent. The "distance" $\tilde{l}$ between the curves $\tilde{x} = \tilde{x}^*(\varepsilon)$, and $\tilde{x} = \tilde{x}_k^*(\varepsilon)$ along the normal is minimal. Its "transparency" can be estimated as $\sim \exp[-\tilde{l}(\tilde{x})]$.

Since the curve $\tilde{x} = \tilde{x}_k^*(\varepsilon)$ is shifted by $\tilde{\varepsilon}_k$ along the $\tilde{\varepsilon}$ axis in respect of $\tilde{x} = \tilde{x}^*(\varepsilon)$, this distance is maximal and equals $\tilde{\varepsilon}_k - \tilde{\varepsilon}_1$ at $\tilde{x} = 0$, and decreases monotonously from discharge center towards its periphery. For a concave potential profile of the type of (15), this rise occurs up to the distance from the wall $(L - x) \geq \lambda_\varepsilon^*$ where the EDF decrease in the region *IIb* compensates the barrier transparency. Accordingly, the $W_k(x)$ maxima are to be rather sharp and situated in the wall vicinity. It illustrates (Fig. 8a) which shows the normed radial profiles of different *Ar* atoms states at p = 6 torr, R = 1 cm, and and I = 3 mA.

It follows from the above discussion that the higher the level, the larger the shift of the peak of the excitation rate profile toward the periphery caused by concerned here effects of EDF nonlocality. But usually the metastable atom density *Nm* is fairly high and stepwise excitation could be more effective than above considered direct excitation from the ground state. In such situation this shift is superimposed by the little known effect of the replication of the slow (nonlocal) part of the EDF in its fast part [9]. In the superelastic collisions with metastable atoms, a slow bulk electron participating in the reaction $Ar^* + e \rightarrow Ar + \vec{e}$ additionally acquires the threshold excitation energy ε^* and instantaneously becomes fast. These processes substantially enhance population of the fast component of the EDF and influence the calculated values of the constants for the excitation reactions with high threshold energies and, accordingly, the densities of highly excited states as it illustrates Fig. 9 (see [9] for details). As was shown in [9] and also can be seen from Fig. 9, the fast components of the EDF ($\varepsilon > \varepsilon^*$) can be represented as a sum $f_0 = f_{0t} + f_{0h}$. If the density N_m of

metastable atoms is high enough, then, the part of the EDF that corresponds to $N_m = 0$ and sharply decreases at energies above the threshold energy ($\varepsilon > \varepsilon^*$),

$$f_{0t}(\varepsilon) \simeq c_{nt} \exp(-\varepsilon / T^*) \qquad (20)$$

is supplemented with a gently sloping pedestal

$$f_{oh}(\varepsilon) \simeq \frac{n_m g_a}{N_0 g_m} f_0(\varepsilon - \varepsilon^*) \qquad (21)$$

replicating the shape of the slow component (the body) of the EDF (here, N_0 is the density of atoms in the ground state). Because of the low effective temperature of the fast electrons T^* (8) the EDF f_{0t} (20) falls rapidly at higher energies and, as early as at energies of a few electronvolts above the threshold ε^*, it is considerably less than the EDF f_{oh} (21) (Fig. 9). Thus, excitation of higher levels can be given by sum of two terms

$$W_k(x) = W_k^d(x) + W_k^{st}(x) \qquad (22)$$

(direct and stepwise).

Since energy dependence of f_{oh} is close to that of the EDF of slow electrons ($\varepsilon < \varepsilon^*$), the spatial profiles of the frequencies and rates of the processes that are determined by these parts of the EDF can also be close to one another [9]. Therefore, when the density N_m is fairly high, the shift on Fig.7a is superimposed by the effect of the replication of the slow (nonlocal) part of the EDF in its fast part (see [9] and Fig. 8b). Therefore, for energies $\varepsilon > \varepsilon_h$, at which the EDF f_{0h} (21) is larger than f_{0t} (20), the effect of the shift of the peak of the excitation rate profile disappears and it should be approach to position of metastable profile maximum. This is illustrated by Fig. 8b. For comparison, Fig. 10 demonstrates the position of the coordinate r_0 corresponding to the peak of the excitation rate profile for the *k-th* level as a function of the energy ε_k of this level. The EDF was calculated with (curve *A*) and without (curve *B*) allowance for impacts of the second kind. It can be seen that curve *B* increases monotonically, while in curve *A*, the effect of the high level peak shift is disappeared because of the increase in the tail of the EDF due to superelastic collisions at high energies. In such situation the high level spatial profiles start to repeat the metastable atoms profile. In other words, for high energy levels direct and stepwise excitations are the two different reasons for nonmonotonic behavior of spatial profiles of excitation rates which superimposed each other (see below Fig.11 and to compear the curves *A* and *F*). In one's turn, to change in practice comparative part one or another it can control the spatial profiles of excitation rates.

In a real situation, some additional affecting factors which were not accounted in kinetic equation (6) can mask the presented effects caused by EDF nonlocality. At increasing the discharge current should be expected the influence of gas temperature heating resulting to decreasing of normal atoms density and electron-electron collisions maxwelliazise EDF. To illustrate their comparative part on Figs.11-15) are shown the simulation results at *p = 7 torr, R = 1 cm* and *I = 30 mA* for different energy excitation: *11.55 eV (a), 12.91 eV (b) and 13.98 eV (c).* The Fig.11a corresponds the metastable level and Fig.11b, corresponds intermediate excited state and Fig.11c corresponds the high energy level. The changing of the corresponding EDF and the profiles of metastable atom densities are presented on Fig.12 and 13. In accordance with made above, superelastic collision don't affect on maximum position of metastable states (see Fig.11a, curves A,F), whereas it influences on position of high energy levels (Fig.11c, curves A,F).

When electron-electron collisions are accounted (curves B on Fig.11-16), for low excited levels the nonmonotonic effect disappears (see Fig.11a, curves B and E). It connected as to change

the profiles of the density and mean energy of the electrons (see Fig.14,15) and, as consequence, decreasing of the ambipolar field (see Fig.16) so the increasing of the EDF tail (see Figs.12). But for higher levels which excitation can be given by sum of two terms (22) (direct and stepwise); therefore at strong electron-electron collisions disappears only stepwise component $W_k^{st}(x)$, whereas direct component $W_k^d(x)$ can create the nonmonotonic profiles (see Fig.11c, curves *B* and *E*).

Gas temperature heating results to decreasing of normal atoms density in the central part of discharge volume. Due to increasing *E/N* parameter, the diffusion on energy in the central part of discharge volume is increasing (the first item in (13,15). Increasing of respectiv energy scale (8) and lengh (5) also play destructive role for existence of being investigated nonmonotonic effect (see Fig.11, curves *C* and *D*).

In more complex systems, such as molecular gases, gas mixtures, DC and RF discharges of more complex geometry, in magnetic field, far more diverse kinetic formation scenaria of the spatial profiles of the excitation rates, as well, as of the luminosity and plasma composition, are to be expected.

In summary, the influence of the nonlocal character of the EDF on the spatial profiles of of excitation rates is essential. A paradoxical effect of shift of the excitation rates, it concise explaination and scalings in a PC at moderate and high pressures are presented.

Acknowledgements.

The work was supported by the CRDF grant # RP1-567-ST-03 and ISTS #3098. Authors also are grateful to R.R.Arslanbekov and V.I.Kolobov for numerous useful discussions.

Figures

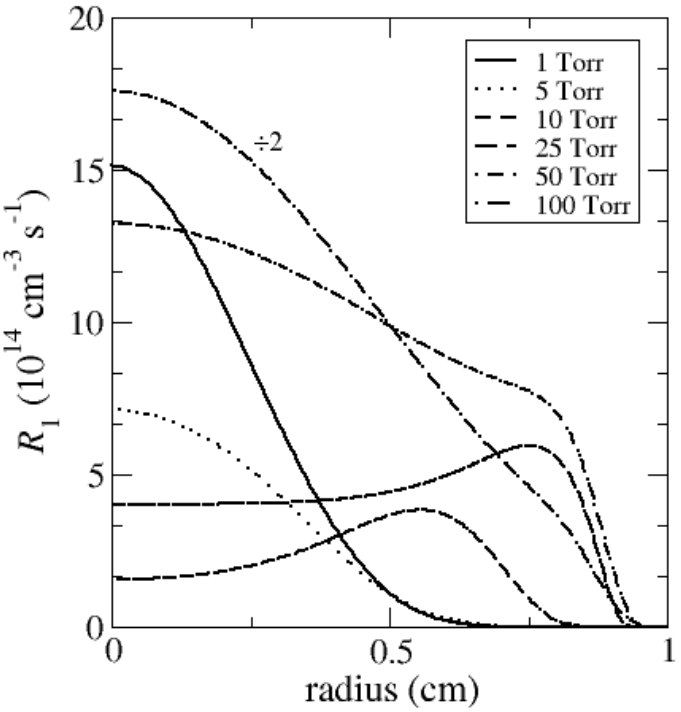

Fig. 1. Radial profiles of excitation rates of Ar* (a) and Ar** (b) at different pressures.

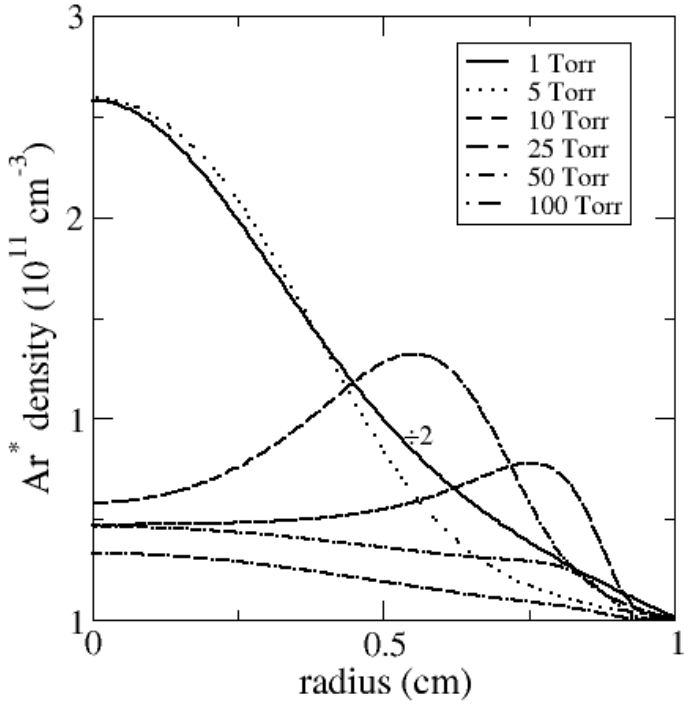

Fig. 2. Radial profiles of excited Ar* species at different pressures.

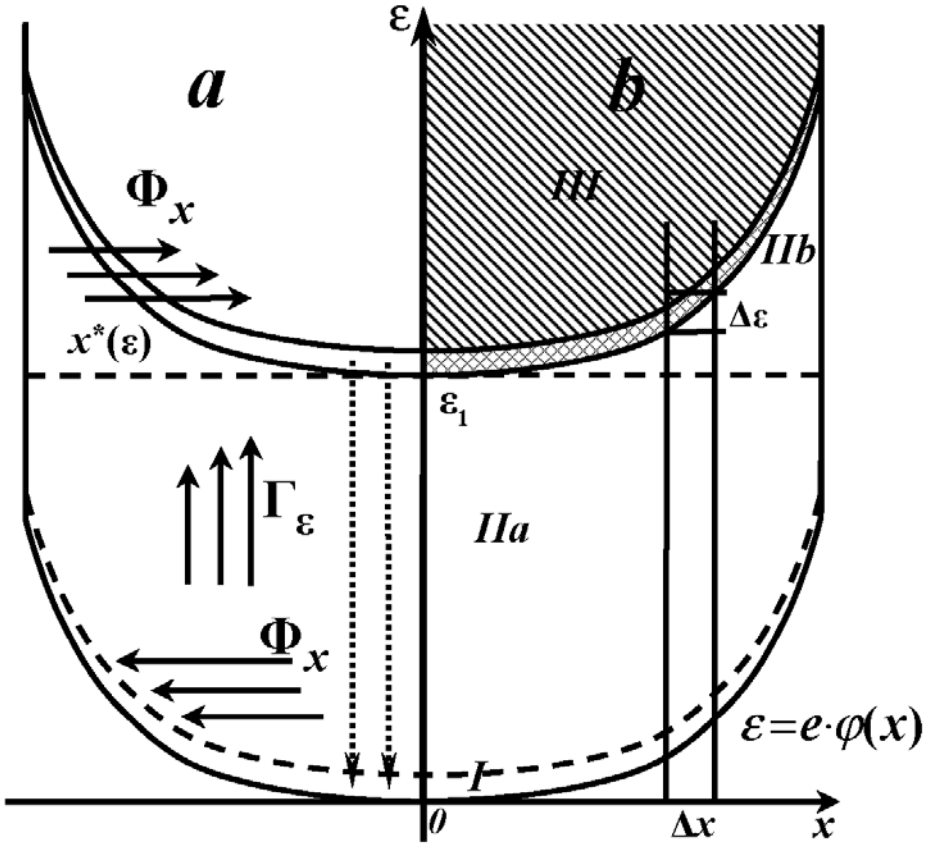

Fig.3: a: Formation scheme of the spatial differential fluxes $\Phi_\varepsilon(x,\varepsilon)$, and of the flux along the energy axis $\Gamma_\varepsilon(x,\varepsilon)$. The dashed arrows relate to the electrons which have lost energy in the inelastic collisions. b. The integration domain of (6) in the (x,ε) plane.

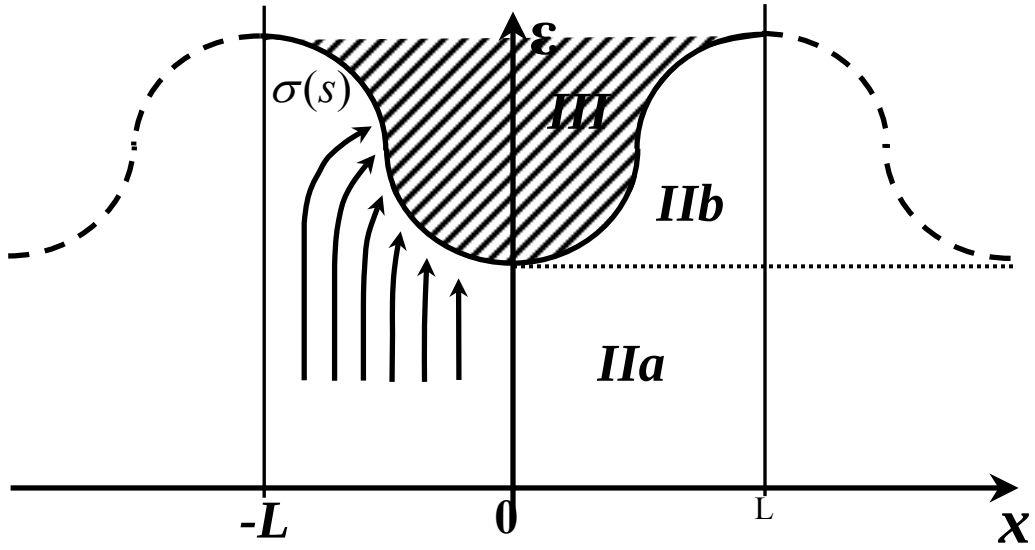

Fig.4. Electrostatic analogy.

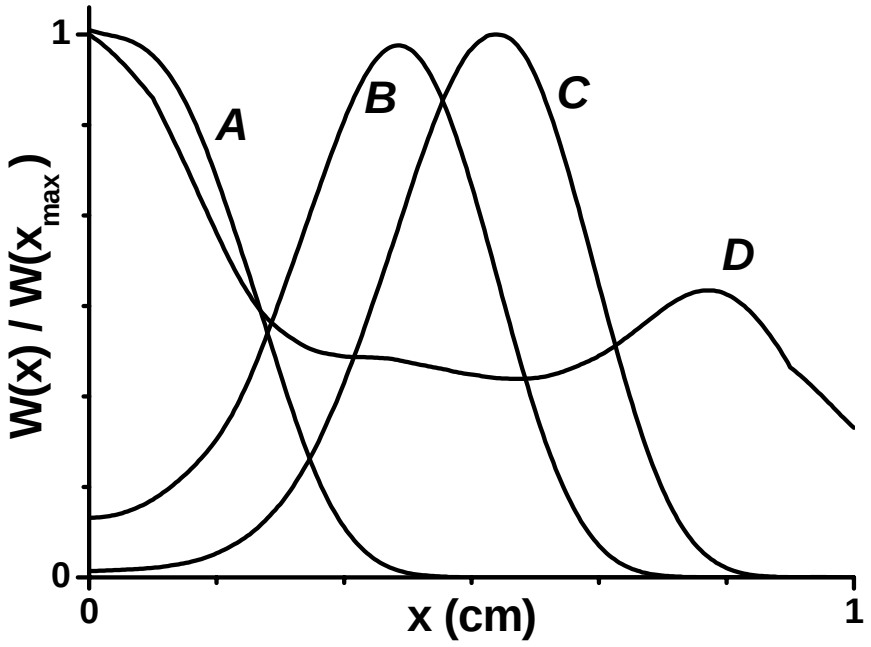

Fig.5. Spatial profiles of the excitation rate for $E_z/p=0.65V/cm$ and $e\varphi(x)=\varepsilon_1(x/L)^3$ for different $p=0.5(A),5(B),\ 10(C)$ and $100(D)$ *Torr*.

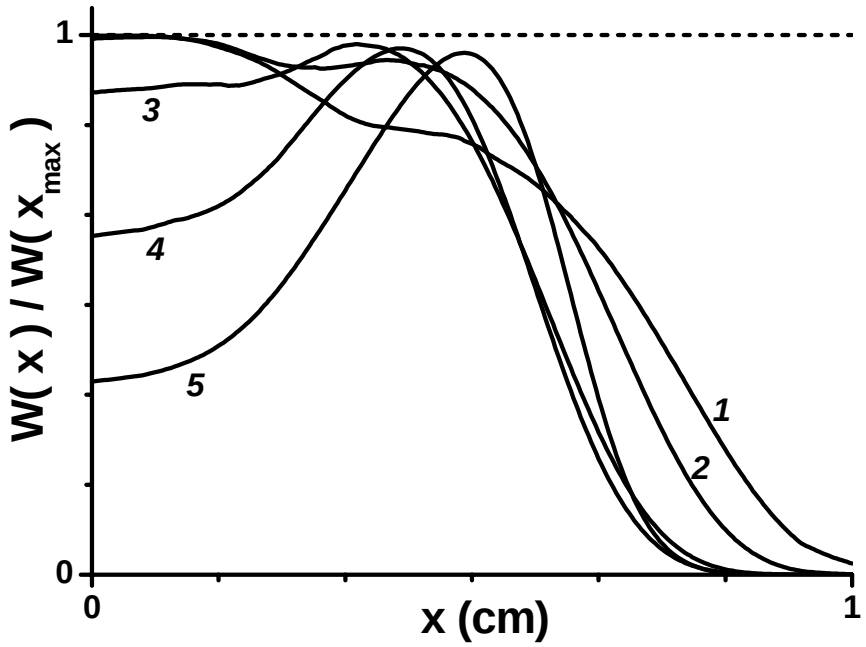

Fig.6. Spatial profiles of the excitation rate for $E_z=5V/cm,\ p=3Torr$ and $e\varphi(x)=\varepsilon_1(x/L)^3$ for different a: *0 (dotted line); 0.25(1); 1(2); 1.5(3).*

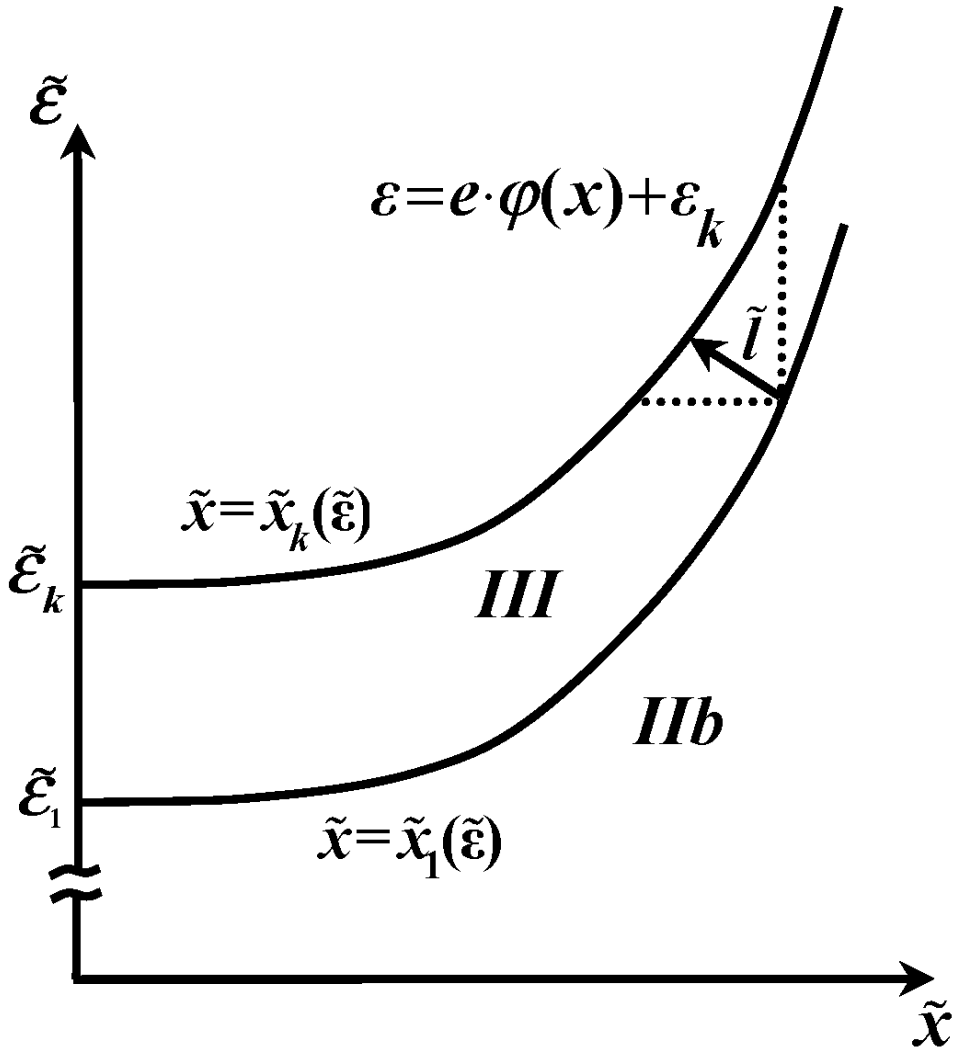

Fig.7. Formation scheme of excitation spatial profiles for high energy levels.

a)

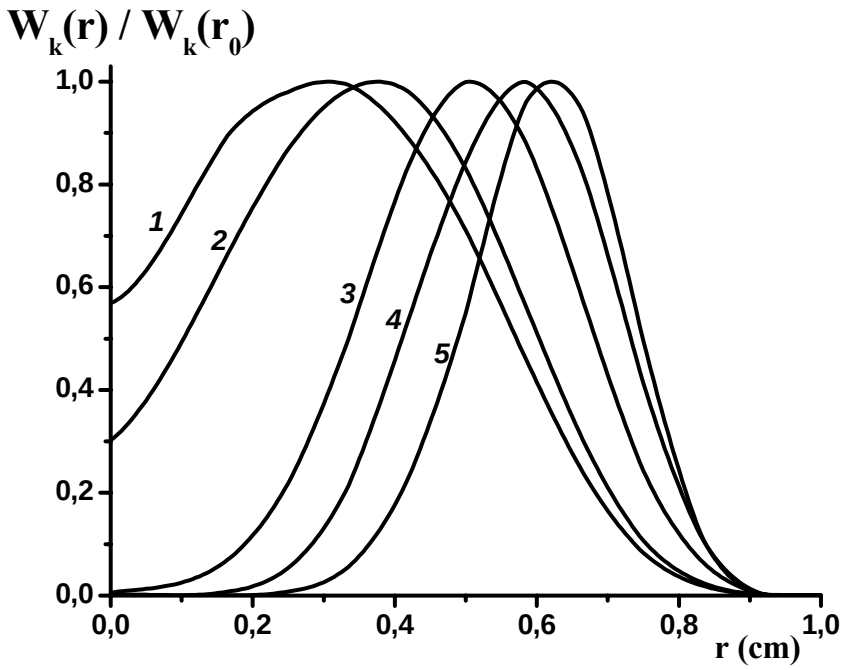

b)

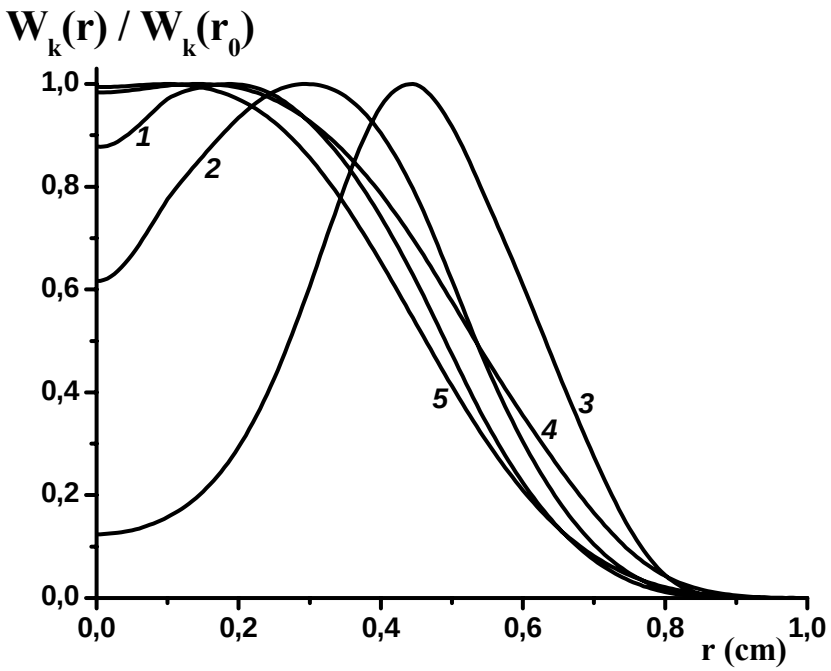

Fig. 8. Profiles of the excitation rates (normalized to their maximum values) of different levels of *argon atoms k = (1) 1, (2) 3, (3) 5, (4) 17, and (5) 25 with energies of* ε_k = 11.55, 11.72, 12.91, 14.01, and *15.2 eV*, respectively, calculated (a) without and (b) with allowance for impacts of the second kind; r_0 is the coordinate of the peak of the excitation rate profile.

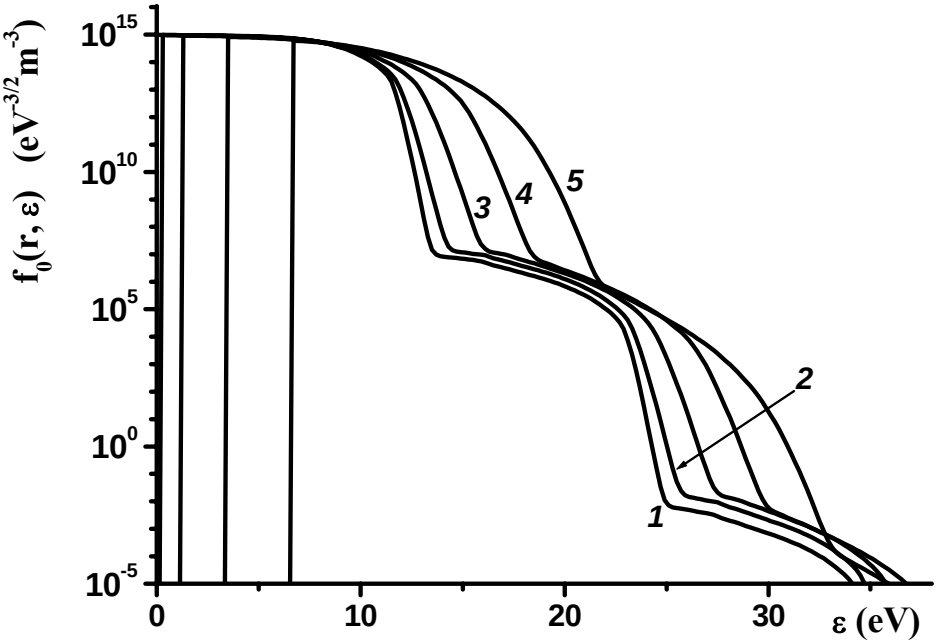

Fig. 9. EDFs at different radii r as functions of the total energy ε:
r = (*1*) 0, (*2*) 0.2R, (*3*) 0.4R, (*4*) 0.6R, and (*5*) 0.8R.

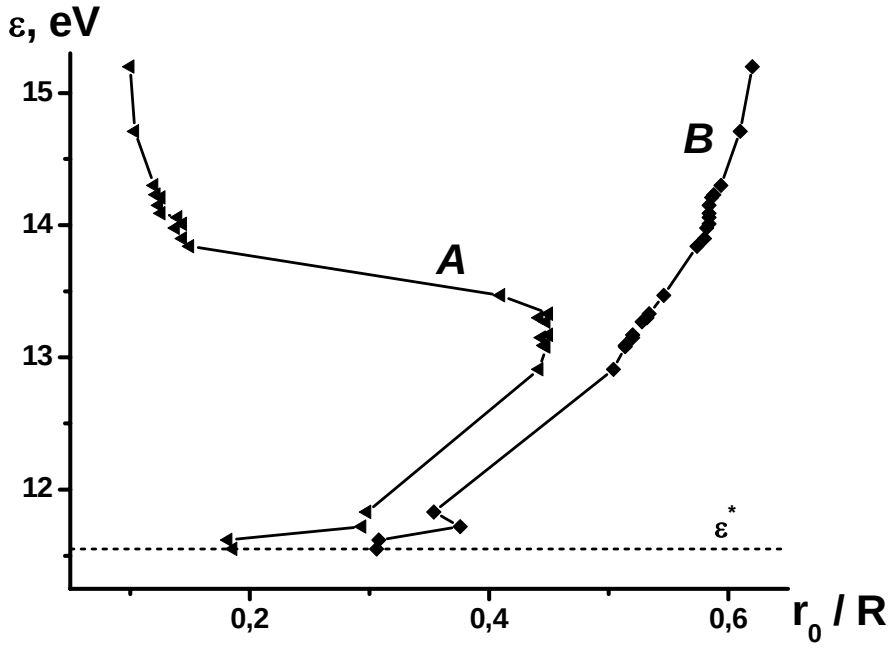

Fig. 10. Coordinate r_0 of the peak of the excitation rate profile for the kth level as a function of the energy ε_k of this level. Curves A and B show the results of calculations with and without allowance for impacts of the second kind, respectively. The dotted line corresponds to the energy of the metastable state.

a)

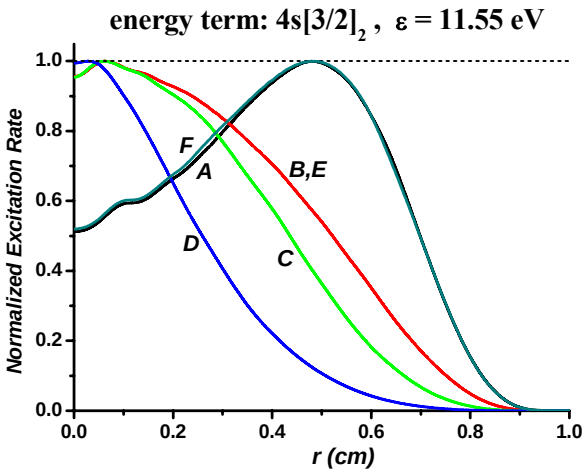

b)

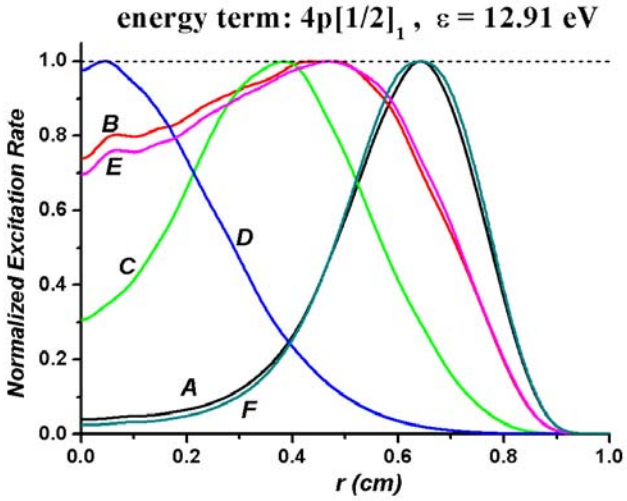

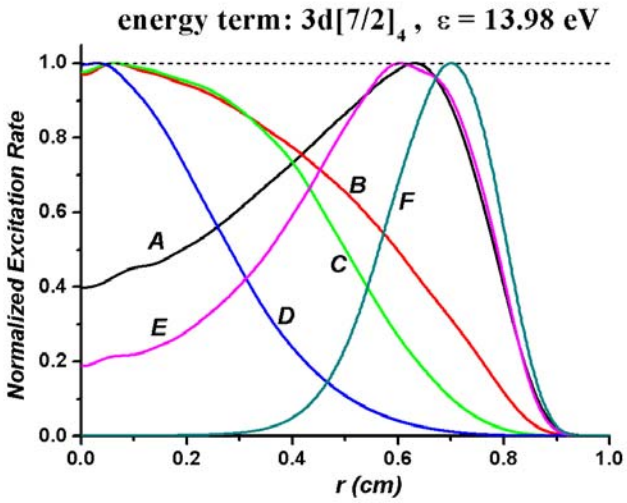

c)

Fig. 11(a-c). Radial excitation rate profiles (normalised on maximal value) for several energy terms of Argon (with k = 1, 5,16). P = 7 Torr, R = 1cm, I=30mA.

A) without account of Coulomb collisions and gas heating;
B) with account of Coulomb collisions, but without account of gas heating;
C) with account gas heating, but without account of Coulomb collisions;
D) with account of Coulomb collisions and gas heating;
E) same as B, but without account of superelastic collisions and Penning ionization processes;
F) without account of Coulomb collisions, gas heating and superelastic collisions.

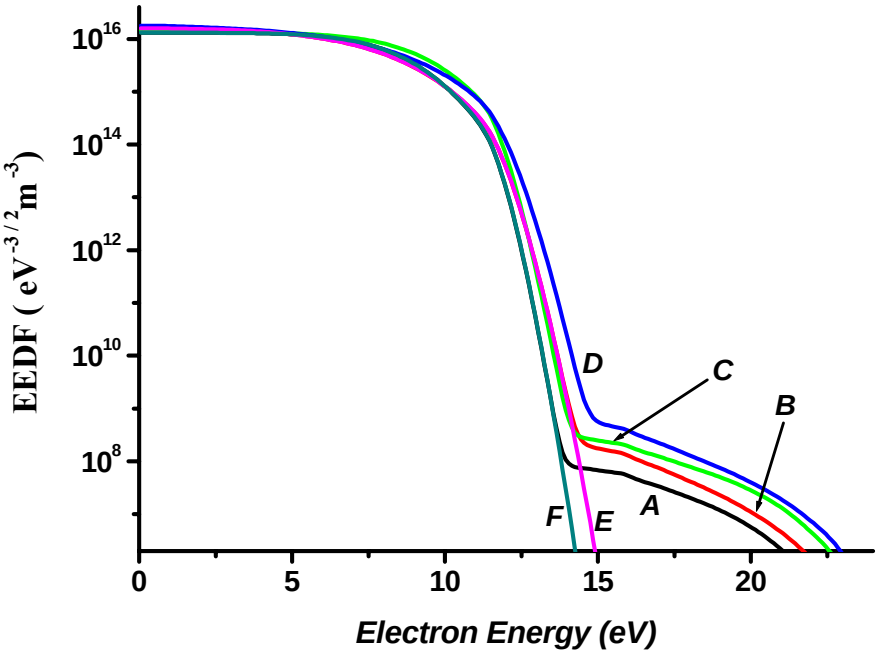

Fig. 12. EEDF on the tube axis. The sense of symbols *A*, *B*, *C*, *D*, *E*, *F* and physical conditions (*P*, *R*, *I*) are same as in Fig.11.

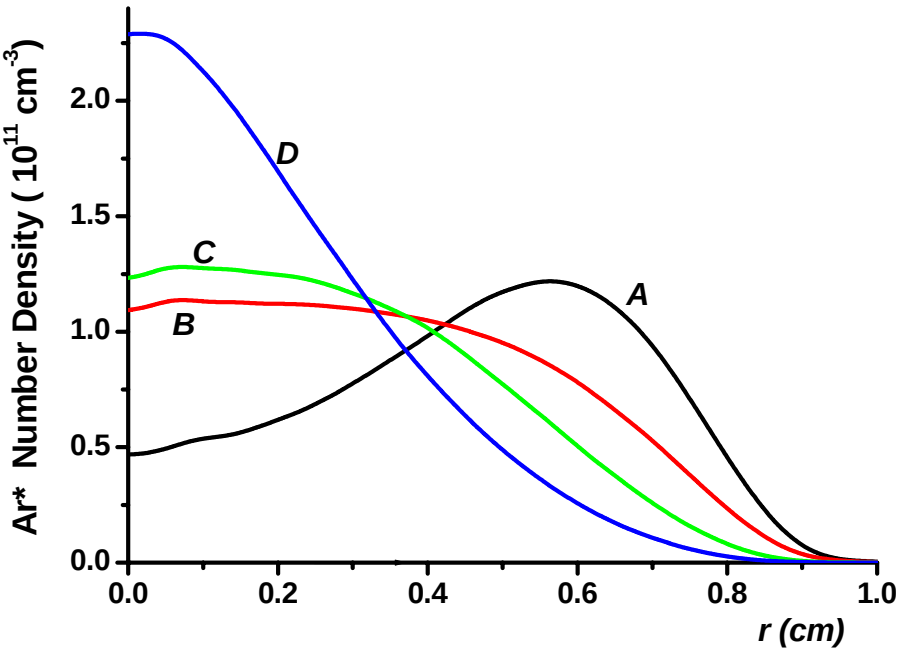

Fig.13. The spatial profiles of the of metastable atoms densities. The sense of symbols *A*, *B*, *C*, *D*, *E*, *F* and physical conditions (*P*, *R*, *I*) are same as in Fig.11.

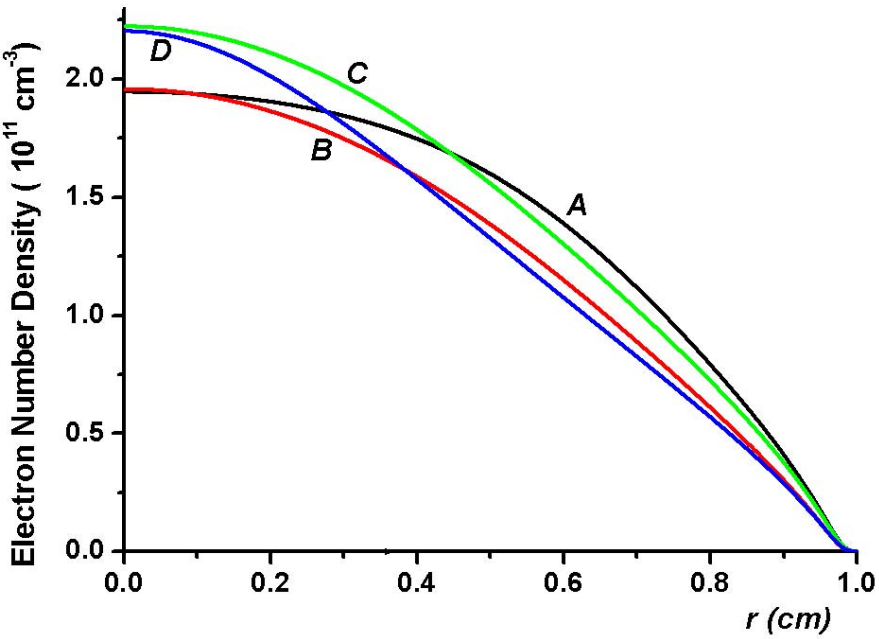

Fig.14. Spatial profiles of the electron density. The sense of symbols *A*, *B*, *C*, *D*, *E*, *F* and physical conditions (*P*, *R*, *I*) are same as in Fig.11.

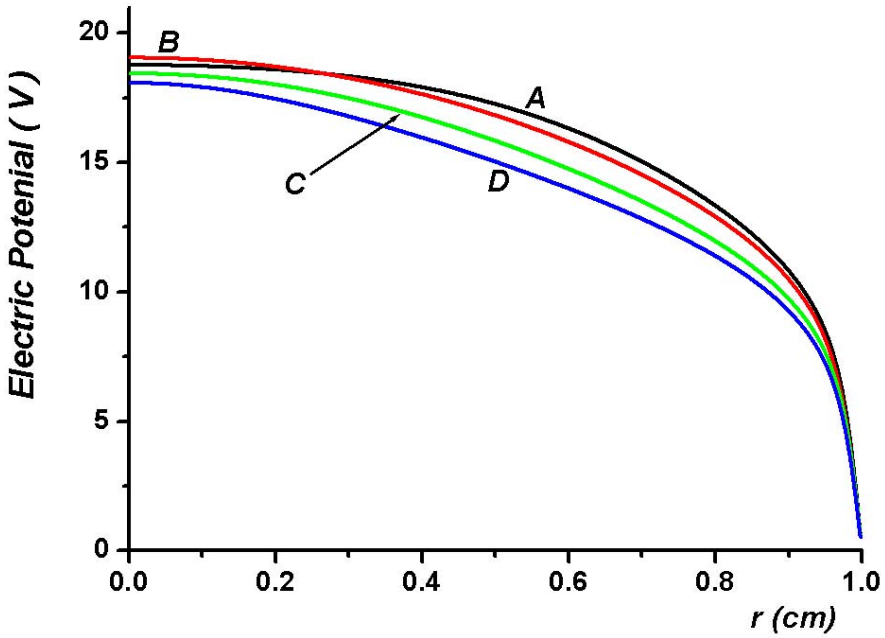

Fig. 15. Spatial profiles of the electric potential. The sense of symbols *A*, *B*, *C*, *D*, *E*, *F* and physical conditions (*P*, *R*, *I*) are same as in Fig.11.

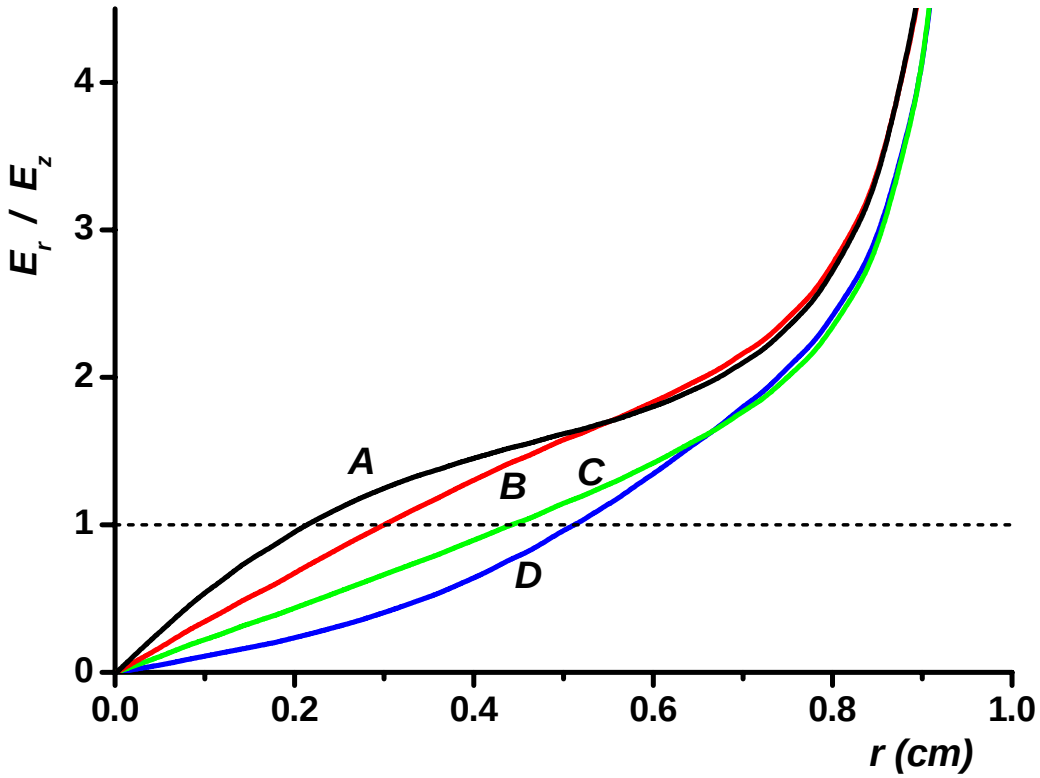

Fig 16. Normalized to E_z profiles of radial electric field E_r. The sense of symbols *A*, *B*, *C*, *D*, *E*, *F* and physical conditions (*P*, *R*, *I*) on Figs 2-5 are same as in Fig.1. Curves *E* and *F* do not presented on Figs 2-4 because curve *E* almost same with curve *B* and curve *F* almost same with curve *A*.

The table of E_z values presented bellow:

#	*A*	*B*	*C*	*D*	*E*	*F*
E_z (V/cm)	8.19	8.02	6.34	6.07	8.02	8.21

References

1. Lieberman M., Lichtenberg A. Principles of Plasma Discharges and Materials Processing. NY, Wiley, 1994.
2. Raizer. Gas Discharge Physics. Spriner-Verlag, 1991.
3. E.M. Lifshitz, L.P. Pitaevsky, Physical Kinetics, Pergamon Press, Oxford (1981).
4. L.D.Tsendin. Plasma Sources, Sci. Technol., v.4, p. 200, 1995.
5. J.Behnke, Yu.Golobovsky, S.U.Nisimov, I.A.Porokhova. Contrib.Plasma.Phys, v.36, p.75, 1996.
6. U. Kortshagen, G.J. Parker, J.E. Lowler. Phys. Rev.E, v.54, p.6746, 1996.

7. G.Mumken, H.Shlueter, L.D.Tsendin. Phys. Rev.E., v.60, p.2250, 1999.
8. E. A. Bogdanov, A. A. Kudryavtsev, L. D. Tsendin, R. R. Arslanbekov, V. I. Kolobov, and V. V. Kudryavtsev. Technical Physics, Vol. 49, No. 6, 2004, pp. 698–706.
9. E. A. Bogdanov, A. A. Kudryavtsev, L. D. Tsendin, R. R. Arslanbekov, V. I. Kolobov. Technical Physics, v.49, No. 7, p. 849–857, 2004.
10. R. R. Arslanbekov, V. I. Kolobov, E. A. Bogdanov, A. A. Kudryavtsev. Appl.Phys.Lett., v.85, N16, p. 3396, 2004.
11. L. D. Tsendin, E. A. Bogdanov, A. A. Kudryavtsev. Physical Review Letters, v.94, N1, p.?, 2005.
12. http://www.cfdrc.com/~cfdplasma.
13. E. A. Bogdanov, A. A. Kudryavtsev, R. R. Arslanbekov, V. I. Kolobov. J.Phys.D:Appl.Phys., v.37, p. 2987-2995, 2004.